J Appl Electrochem (2009) 39:807–814
DOI 10.1007/s10800-008-9725-x

ORIGINAL PAPER

Electrochemical properties of $LiNi_{1-y}M_yO_2$ (M=Ni, Ga, Al and/or Ti) cathodes synthesized by the combustion method

Myoung Youp Song · Sung Nam Kwon · Soon-Do Yoon · Daniel R. Mumm

Received: 7 October 2008 / Accepted: 6 November 2008 / Published online: 28 November 2008

Abstract $LiNiO_2$, $LiNi_{0.995}Al_{0.005}O_2$, $LiNi_{0.975}Ga_{0.025}O_2$, $LiNi_{0.990}Ti_{0.010}O_2$ and $LiNi_{0.990}Al_{0.005}Ti_{0.005}O_2$ were synthesized by preheating at 400 °C for 30 min in air and calcination at 750 °C for 36 h in an O_2 stream with excess lithium amount $z = 0.10$ in $Li_{1+z}Ni_{1-y}M_yO_2$. For these samples, the discharge capacities and discharge capacity degradation rate are compared. $LiNiO_2$ has the largest discharge capacity at the 20th cycle ($n = 20$) and the 50th cycle ($n = 50$). $LiNiO_2$ and $LiNi_{0.995}Al_{0.005}O_2$ have relatively good cycling performances and their discharge capacities at $n = 50$ are 134 and 123 mAh/g, respectively, at 0.1 C rate. The crystallite sizes and strains were calculated by the Williamson–Hall method with XRD patterns and compared for the samples as prepared and after 50 charge–discharge cycles.

M. Y. Song (✉)
Division of Advanced Materials Engineering, Nanomaterials Processing Research Center, Engineering Research Institute, Chonbuk National University, 664-14 Deogjindong 1-ga, Deogjingu, Jeonju 561-756, Republic of Korea
e-mail: songmy@chonbuk.ac.kr

S. N. Kwon
Department of Hydrogen and Fuel Cells Engineering, Specialized Graduate School, Chonbuk National University, 664-14 Deogjindong 1-ga, Deogjingu, Jeonju 561-756, Republic of Korea

S.-D. Yoon
School of Applied Chemical Engineering, Chonnam National University, 300 Yongbongdong Bukgu, Gwangju 500-757, Republic of Korea

D. R. Mumm
Department of Chemical Engineering and Materials Science, University of California, Irvine, CA 92697-2575, USA

Keywords $LiNi_{1-y}M_yO_2$ (M=Ni, Ga, Al and/or Ti) · Combustion method · Electrochemical properties · I_{003}/I_{104} · R-factor

1 Introduction

Transition metal oxides such as $LiMn_2O_4$ [1–3], $LiCoO_2$ [4–6], and $LiNiO_2$ [7–10] have been intensively investigated in order to use them as the cathode materials of lithium secondary batteries. $LiMn_2O_4$ is comparatively inexpensive and does not bring about any environmental pollution, but its cycling performance is not adequate. $LiCoO_2$ has a large diffusivity and a high operating voltage, and it can be easily prepared. However, it has the disadvantage that it contains Co, an expensive element. $LiNiO_2$ is a very promising cathode material since it has a large discharge capacity [11] and is excellent from the economic and environmental viewpoints. On the other hand, its preparation is very difficult compared with $LiCoO_2$ and $LiMn_2O_4$.

It is known that $Li_{1-x}Ni_{1+x}O_2$ forms rather than the stoichiometric $LiNiO_2$ during preparation [12] due to cation mixing. Excess nickel occupies the Li sites, destroying the ideally layered structure and preventing the lithium ions from undergoing the easy movement required for intercalation and deintercalation during cycling. This results in a small discharge capacity and poor cycling performance.

To improve the electrochemical properties of $LiNiO_2$, Co [13], Al [14, 15], Ti [16], Ga [11], Mn [17] and Fe [18, 19] were substituted for nickel by the synthesis in oxygen. Guildmard et al. [14] investigated the electrochemical performances of $LiNi_{1-y}Al_yO_2$ ($0.10 \leq y \leq 0.50$) specimens synthesized by a co-precipitation method. They showed that aluminum substitution suppressed all the phase

transitions observed for the $LiNiO_2$ system. Chang et al. [16] detected partial disordering between the transition metal (Ni and Ti) layer and lithium by Rietveld refinement in $Li_xNi_{1-y}Ti_yO_2$ ($0.1 \leq y \leq 0.5$) prepared by solid state reaction. By considering the ionic radius and the Ni–O bond length, they concluded that the Ni(II) ions are partially stabilized in the lithium sites. Nishida et al. [11] reported that gallium-doping into $LiNiO_2$ stabilizes the crystal structure during the charging process and leads to better cycling performance than $LiNiO_2$.

$LiNiO_2$ synthesized by the solid-state reaction method does not have a high discharge capacity and has poor cycling performance, probably because it has poor crystallinity and non-uniform particle size. On the other hand, homogeneous mixing of the starting materials is possible in the combustion method because the starting materials are liquid. This may lead to good crystallinity and uniform particle size.

In this work, $LiNi_{1-y}M_yO_2$ (M=Ni, Ga, Al and/or Ti) specimens were synthesized by the combustion method, and the electrochemical properties of the synthesized samples were investigated.

2 Experimental

$LiNiO_2$, $LiNi_{0.995}Al_{0.005}O_2$, $LiNi_{0.975}Ga_{0.025}O_2$, $LiNi_{0.990}Ti_{0.010}O_2$ and $LiNi_{0.990}Al_{0.005}Ti_{0.005}O_2$ were synthesized by the combustion method. These compositions were chosen because the specimens with these compositions had relatively good electrochemical properties in our previous works [20, 21]. Aldrich Chemical's $LiNO_3$, $Ni(NO_3)_2 \cdot 6H_2O$, $Al(NO_3)_3 \cdot 9H_2O$, $Ga(NO_3)_3 \cdot xH_2O$ and $Ti(NO_3)_4$ were used as starting materials. Excess lithium was added to compensate for the evaporated lithium during preparation. The excess lithium amount z in $Li_{1+z}Ni_{1-y}M_yO_2$ was 0.10. The starting materials, in the desired proportions, were dissolved in distilled water and mixed with urea by a magnetic stirrer. The mole ratio of urea to nitrate was 3.6. The mixture was heated to 400 °C in air and the temperature 400 °C was maintained for 30 min. During that time the mixture formed ash by a combustion reaction. The ash was then pelletized and calcined at 750 °C for 36 h in an O_2 stream. The heating and cooling rates were about 100 °C h^{-1}. These synthesis conditions are the optimum ones to synthesize $LiNiO_2$ by the combustion method, studied in our previous work [22].

The phase identification of the synthesized samples was carried out by X-ray diffraction analysis using CuK_α radiation. A Rigaku III/A X-ray diffractometer was used. The scanning rate was 6 min^{-1} and the scanning range of diffraction angel (2θ) was $10° \leq 2\theta \leq 80°$. The morphologies of the samples were observed by scanning electron microscopy (SEM).

To measure the electrochemical properties, the electrochemical cells consisted of the prepared sample as a positive electrode, Li metal as a negative electrode and an electrolyte of 1 M $LiPF_6$ in a 1:1 (volume ratio) mixture of ethylene carbonate (EC) and diethyl carbonate (DEC). A Whatman glass fiber was used as a separator. The cells were assembled in an argon-filled dry box. To fabricate the positive electrode, active material, acetylene black and polyvinylidene fluoride (PVDF) binder dissolved in *N*-methyl-2-pyrrolidone (NMP) were mixed in a weight ratio 85:10:5 and applied on Al foil. All the electrochemical tests were performed at room temperature with a battery charge–discharge cycle tester at 0.1 C in a potential range from 2.7 to 4.4 V.

3 Results and discussion

Figure 1 shows the XRD patterns of $LiNiO_2$, $LiNi_{0.995}Al_{0.005}O_2$, $LiNi_{0.975}Ga_{0.025}O_2$, $LiNi_{0.990}Ti_{0.010}O_2$ and $LiNi_{0.990}Al_{0.005}Ti_{0.005}O_2$ synthesized by the combustion method with excess lithium amount $y = 0.10$. All the samples have the α-$NaFeO_2$ structure of the rhombohedral system (space group; $R\bar{3}m$) with no evidence of impurities.

Ohzuku et al. [23] reported that the electrochemically reactive $LiNiO_2$ showed larger integrated intensity ratio of 003 peak to 104 peak (I_{003}/I_{104}) and a clear split of the 108 and 110 peaks in their XRD patterns. The degree of cation mixing (displacement of nickel and lithium ions) is low if the value of I_{003}/I_{104} is large and the 108 and 110 peaks are split clearly. The value of $(I_{006} + I_{102})/I_{101}$, called the R-factor, is known to be smaller as the unit cell volume of $Li_yNi_{2-y}O_2$ gets smaller. The R-factor increases as y in $Li_yNi_{2-y}O_2$ decreases for y near 1. This indicates that the R-factor increases as the degree of cation mixing becomes larger [7].

The cation mixing in layered materials makes sliding between basal planes impossible, resulting in electrochemical inactivity [23]. Hexagonal ordering implies good layered structure which has a characteristic property of sliding between basal planes. High cation mixing thus corresponds to low hexagonal ordering. A Large R-factor, which increases with the degree of cation mixing, indicates low hexagonal ordering.

Table 1 gives the lattice parameters a, c, c/a, unit cell volume, I_{003}/I_{104} and R-factor calculated from XRD patterns of the materials synthesized with excess lithium amount $y = 0.10$.

$LiNiO_2$ has the largest value of I_{003}/I_{104}, and decreases in the order of $LiNi_{0.995}Al_{0.005}O_2$, $LiNi_{0.975}Ga_{0.025}O_2$, $LiNi_{0.990}Al_{0.005}Ti_{0.005}O_2$ and $LiNi_{0.990}Ti_{0.010}O_2$. $LiNiO_2$ has the smallest value of R-factor, and increases in the order of $LiNi_{0.990}Ti_{0.010}O_2$, $LiNi_{0.990}Al_{0.005}Ti_{0.005}O_2$,

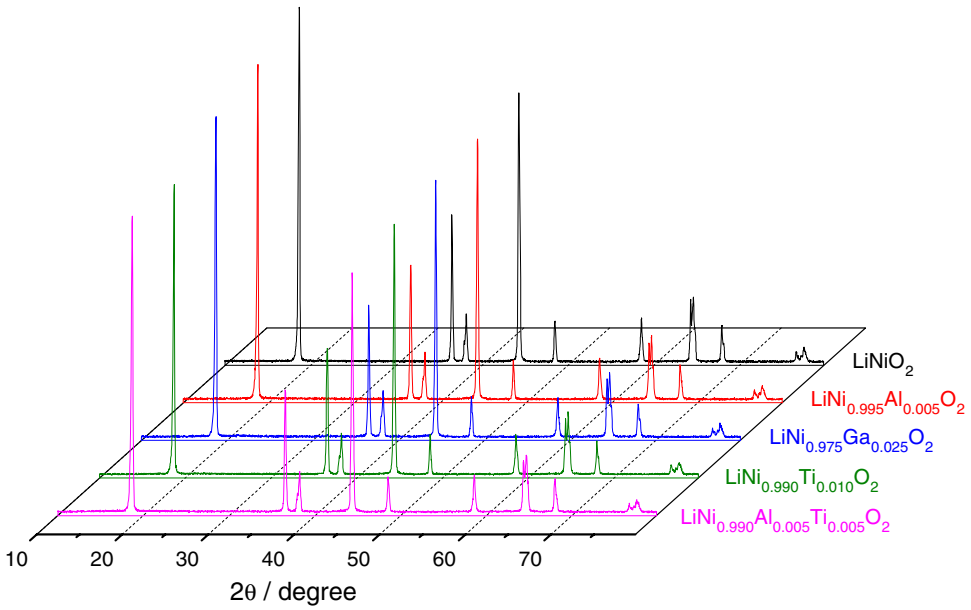

Fig. 1 XRD patterns for the materials synthesized with excess lithium amount $z = 0.10$; $LiNiO_2$, $LiNi_{0.995}Al_{0.005}O_2$, $LiNi_{0.975}Ga_{0.025}O_2$, $LiNi_{0.990}Ti_{0.010}O_2$ and $LiNi_{0.990}Al_{0.005}Ti_{0.005}O_2$

Table 1 Values of a, c, c/a, unit cell volume, I_{003}/I_{104} and R-factor for the materials synthesized with excess lithium amount $z = 0.10$

	a/Å	c/Å	c/a	Unit cell volume/Å^3	I_{003}/I_{104}	R-factor $[(I_{006} + I_{102})/I_{101}]$
$LiNiO_2$	2.881	14.209	4.932	102.146	1.319	0.459
$LiNi_{0.995}Al_{0.005}O_2$	2.880	14.205	4.931	102.067	1.287	0.505
$LiNi_{0.975}Ga_{0.025}O_2$	2.881	14.204	4.930	102.102	1.249	0.498
$LiNi_{0.990}Ti_{0.010}O_2$	2.881	14.209	4.932	102.146	1.160	0.470
$LiNi_{0.990}Al_{0.005}Ti_{0.005}O_2$	2.880	14.208	4.934	102.027	1.236	0.475

$LiNi_{0.975}Ga_{0.025}O_2$ and $LiNi_{0.995}Al_{0.005}O_2$. $LiNiO_2$ has the largest value of I_{003}/I_{104} and the smallest value of R-factor.

Figure 2 shows SEM images of $LiNiO_2$, $LiNi_{0.995}Al_{0.005}O_2$, $LiNi_{0.975}Ga_{0.025}O_2$, $LiNi_{0.990}Ti_{0.010}O_2$ and $LiNi_{0.990}Al_{0.005}Ti_{0.005}O_2$ synthesized with excess lithium amount $y = 0.10$. The particle size decreases in the order of $LiNi_{0.975}Ga_{0.025}O_2$, $LiNiO_2$, $LiNi_{0.995}Al_{0.005}O_2$, $LiNi_{0.990}Ti_{0.010}O_2$ and $LiNi_{0.990}Al_{0.005}Ti_{0.005}O_2$. $LiNi_{0.990}Ti_{0.010}O_2$ and $LiNi_{0.990}Al_{0.005}Ti_{0.005}O_2$ have spherical shape and homogeneous particle size distribution. And $LiNi_{0.990}Al_{0.005}Ti_{0.005}O_2$ has very fine particles.

Figure 3 shows the Coulombic efficiencies of the samples $LiNiO_2$, $LiNi_{0.995}Al_{0.005}O_2$, $LiNi_{0.975}Ga_{0.025}O_2$, $LiNi_{0.990}Ti_{0.010}O_2$ and $LiNi_{0.990}Al_{0.005}Ti_{0.005}O_2$ at 0.1 C rate for the first cycle. $LiNi_{0.990}Ti_{0.010}O_2$ showed the highest Coulombic efficiency (80.5%), and that of $LiNiO_2$ was also high (79.3%). It decreases in the order of $LiNi_{0.990}Al_{0.005}Ti_{0.005}O_2$ (75.0%), $LiNi_{0.995}Al_{0.005}O_2$ (73.2%) and $LiNi_{0.975}Ga_{0.025}O_2$ (68.4%).

Figure 4 shows the variation of the discharge capacity at 0.1 C rate with the number of cycles for the samples $LiNiO_2$, $LiNi_{0.995}Al_{0.005}O_2$, $LiNi_{0.975}Ga_{0.025}O_2$, $LiNi_{0.990}Ti_{0.010}O_2$ and $LiNi_{0.990}Al_{0.005}Ti_{0.005}O_2$. $LiNi_{0.990}Al_{0.005}Ti_{0.005}O_2$ has the largest first discharge capacity, and decreases in the order of $LiNi_{0.990}Ti_{0.010}O_2$, $LiNi_{0.995}Al_{0.005}O_2$, $LiNiO_2$ and $LiNi_{0.975}Ga_{0.025}O_2$. $LiNiO_2$ and $LiNi_{0.995}Al_{0.005}O_2$ have a good cycling performance and their discharge capacities at $n = 50$ are 134, 123 mAh/g. And $LiNi_{0.990}Al_{0.005}Ti_{0.005}O_2$ has the worst cycling performance.

Figure 5 shows the variation of the first discharge capacity, and the discharge capacity at $n = 20$ and $n = 50$ at 0.1 C rate with sample $LiNiO_2$, $LiNi_{0.995}Al_{0.005}O_2$, $LiNi_{0.975}Ga_{0.025}O_2$, $LiNi_{0.990}Ti_{0.010}O_2$ and $LiNi_{0.990}Al_{0.005}Ti_{0.005}O_2$ synthesized with excess lithium amount $y = 0.10$. $LiNi_{0.990}Al_{0.005}Ti_{0.005}O_2$ has the largest first discharge capacity and the first discharge capacity decreases in the order of $LiNi_{0.990}Ti_{0.010}O_2$, $LiNi_{0.995}Al_{0.005}O_2$, $LiNiO_2$ and $LiNi_{0.975}Ga_{0.025}O_2$. $LiNiO_2$ has the largest discharge capacity at $n = 20$ and $n = 50$, they decrease in the order of $LiNi_{0.995}Al_{0.005}O_2$, $LiNi_{0.975}Ga_{0.025}O_2$, $LiNi_{0.990}Ti_{0.010}O_2$ and $LiNi_{0.990}Al_{0.005}Ti_{0.005}O_2$.

Figure 6 shows the variation of the discharge capacity degradation rates for $n = 1$–20 (between $n = 1$ and $n = 20$) and for $n = 21$–50 (between $n = 21$ and $n = 50$) at 0.1 C rate with the sample $LiNiO_2$, $LiNi_{0.995}Al_{0.005}O_2$, $LiNi_{0.975}Ga_{0.025}O_2$, $LiNi_{0.990}Ti_{0.010}O_2$ and $LiNi_{0.990}Al_{0.005}Ti_{0.005}O_2$. $LiNi_{0.975}Ga_{0.025}O_2$ has the smallest discharge

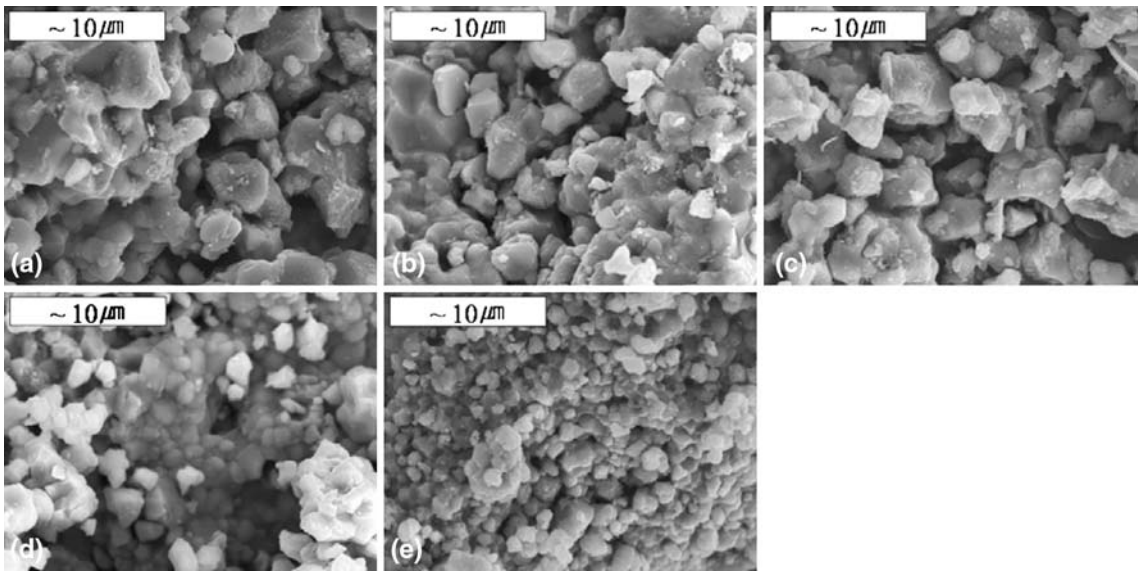

Fig. 2 SEM images of the materials synthesized with excess lithium amount $z = 0.10$; (**a**) $LiNiO_2$, (**b**) $LiNi_{0.995}Al_{0.005}O_2$, (**c**) $LiNi_{0.975}Ga_{0.025}O_2$, (**d**) $LiNi_{0.990}Ti_{0.010}O_2$ and (**e**) $LiNi_{0.990}Al_{0.005}Ti_{0.005}O_2$

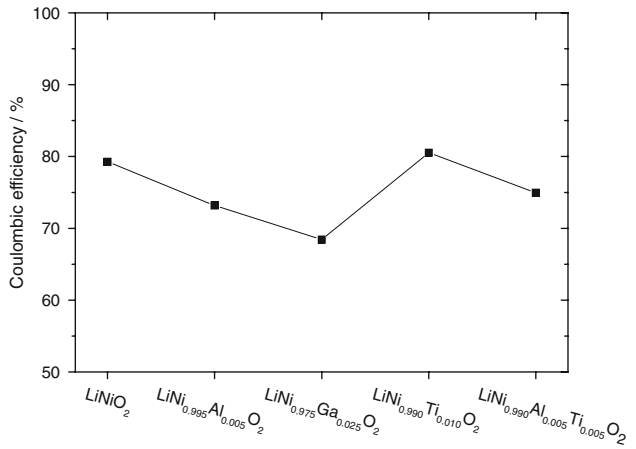

Fig. 3 Coulombic efficiencies of the samples $LiNiO_2$, $LiNi_{0.995}Al_{0.005}O_2$, $LiNi_{0.975}Ga_{0.025}O_2$, $LiNi_{0.990}Ti_{0.010}O_2$ and $LiNi_{0.990}Al_{0.005}Ti_{0.005}O_2$ at 0.1 C rate for the first cycle

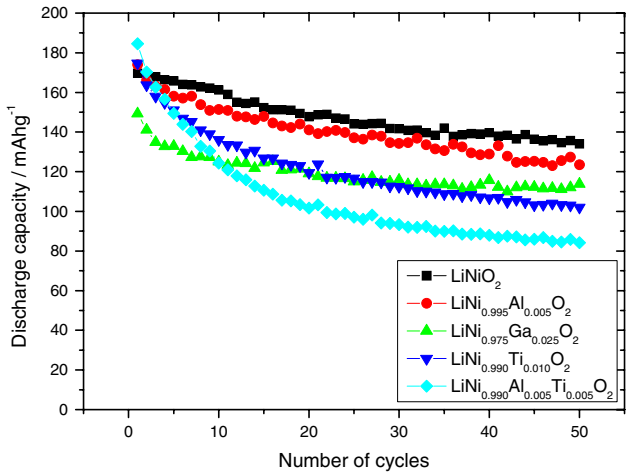

Fig. 4 Variation of the discharge capacity at 0.1 C rate with the number of cycles for the samples $LiNiO_2$, $LiNi_{0.995}Al_{0.005}O_2$, $LiNi_{0.975}Ga_{0.025}O_2$, $LiNi_{0.990}Ti_{0.010}O_2$ and $LiNi_{0.990}Al_{0.005}Ti_{0.005}O_2$

capacity degradation rates for $n = 1$–20 and for $n = 21$–50. They increase in the order of $LiNiO_2$, $LiNi_{0.995}Al_{0.005}O_2$, $LiNi_{0.990}Ti_{0.010}O_2$ and $LiNi_{0.990}Al_{0.005}Ti_{0.005}O_2$. The variation of the first discharge capacity with the sample has a similar trend to that of the discharge capacity degradation rate with the samples. This shows that the sample with a large first discharge capacity has a large discharge capacity degradation rate. $LiNiO_2$ and $LiNi_{0.995}Al_{0.005}O_2$ have a relatively good cycling performance and their discharge capacities at $n = 50$ are 134, 123 mAh/g at 0.1 C rate.

Figure 7 shows the variations of I_{003}/I_{104} and R-factor with the synthesized samples. It is hard to find out some relationship of the variation of R-factor with those of the first discharge capacity, the discharge capacities at $n = 20$ and $n = 50$, and the discharge capacity degradation rates. But as the value of I_{003}/I_{104} increases, roughly speaking, the discharge capacity degradation rate decreases and the discharge capacities at $n = 20$ and $n = 50$ increase.

Figure 8 shows the XRD patterns after 50 charge–discharge cycles at 0.1 C rate of the materials synthesized with excess lithium amount $y = 0.10$. All the samples have the α-$NaFeO_2$ structure of the rhombohedral system (space group; $R\bar{3}m$) with no evidence of impurities.

Table 2 gives the lattice parameters a, c, c/a, unit cell volume, I_{003}/I_{104} and R-factor calculated from XRD patterns after 50 charge–discharge cycles at 0.1 C rate of the materials synthesized with excess lithium amount

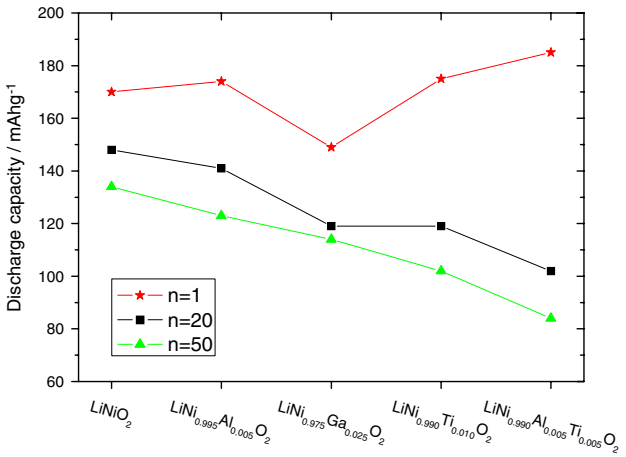

Fig. 5 Variation of the first discharge capacity, and the discharge capacity at $n = 20$ and $n = 50$ at 0.1 C rate with the sample $LiNiO_2$, $LiNi_{0.995}Al_{0.005}O_2$, $LiNi_{0.975}Ga_{0.025}O_2$, $LiNi_{0.990}Ti_{0.010}O_2$ and $LiNi_{0.990}Al_{0.005}Ti_{0.005}O_2$

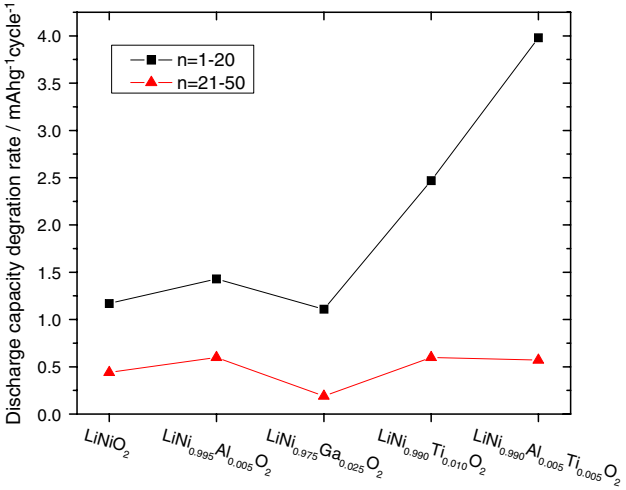

Fig. 6 Variation of the discharge capacity degradation rates for $n = 1$–20 (between $n = 1$ and $n = 20$) and for $n = 21$–50 (between $n = 21$ and $n = 50$) at 0.1 C rate with the sample $LiNiO_2$, $LiNi_{0.995}Al_{0.005}O_2$, $LiNi_{0.975}Ga_{0.025}O_2$, $LiNi_{0.990}Ti_{0.010}O_2$ and $LiNi_{0.990}Al_{0.005}Ti_{0.005}O_2$

$y = 0.10$. $LiNi_{0.995}Al_{0.005}O_2$ has the largest value of I_{003}/I_{104} and decreases in the order of $LiNi_{0.975}Ga_{0.025}O_2$, $LiNiO_2$, $LiNi_{0.990}Ti_{0.010}O_2$ and $LiNi_{0.990}Al_{0.005}Ti_{0.005}O_2$. $LiNi_{0.990}Ti_{0.010}O_2$ has the smallest value of R-factor and increases in the order of $LiNiO_2$, $LiNi_{0.990}Al_{0.005}Ti_{0.005}O_2$, $LiNi_{0.975}Ga_{0.025}O_2$ and $LiNi_{0.995}Al_{0.005}O_2$.

Figure 9 shows the SEM images after 50 charge–discharge cycles of $LiNiO_2$, $LiNi_{0.995}Al_{0.005}O_2$, $LiNi_{0.975}Ga_{0.025}O_2$, $LiNi_{0.990}Ti_{0.010}O_2$ and $LiNi_{0.990}Al_{0.005}Ti_{0.005}O_2$ synthesized with excess lithium amount $y = 0.10$. The particle size decreases in the order of $LiNi_{0.975}Ga_{0.025}O_2$, $LiNiO_2$, $LiNi_{0.995}Al_{0.005}O_2$, $LiNi_{0.990}Ti_{0.010}O_2$ and $LiNi_{0.990}Al_{0.005}Ti_{0.005}O_2$. The shapes of $LiNi_{0.990}Ti_{0.010}O_2$ and $LiNi_{0.990}Al_{0.005}Ti_{0.005}O_2$ are spherical and their particle size

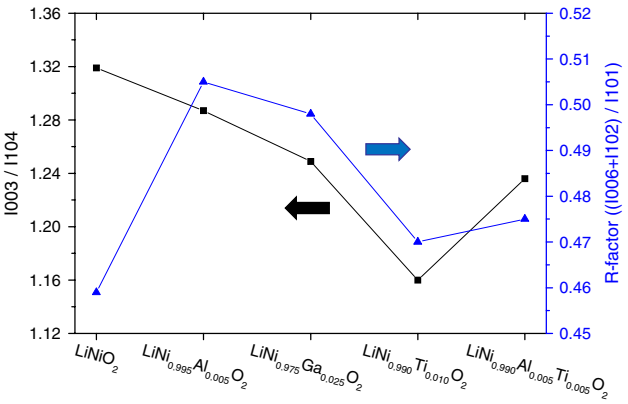

Fig. 7 Variations of I_{003}/I_{104} and R-factor with the synthesized samples

distributions are homogeneous. The particle size of $LiNi_{0.990}Al_{0.005}Ti_{0.005}O_2$ is very fine. The particle sizes of the samples after $n = 50$ are smaller than those before charge–discharge cycling. In particular, the edges of $LiNiO_2$, $LiNi_{0.995}Al_{0.005}O_2$ and $LiNi_{0.975}Ga_{0.025}O_2$ became sharper as compared with the samples before cycling. Cracks are observed on the agglomerates of the particles of $LiNi_{0.990}Ti_{0.010}O_2$.

In order to calculate the crystallite size and the strain of the samples $LiNiO_2$, $LiNi_{0.995}Al_{0.005}O_2$, $LiNi_{0.975}Ga_{0.025}O_2$, $LiNi_{0.990}Ti_{0.010}O_2$ and $LiNi_{0.990}Al_{0.005}Ti_{0.005}O_2$ as synthesized and after 50 charge–discharge cycles, the Williamson–Hall method [24] is applied in which the following equation was used;

$$B\cos\theta = K\lambda/t + 4\varepsilon\sin\theta \quad (1)$$

where B is full width at half maximum, K shape factor (0.9), λ wavelength (1.54056 Å), t crystallite size and ε strain.

Figure 10 shows the variations of the crystallite size with the sample $LiNiO_2$, $LiNi_{0.995}Al_{0.005}O_2$, $LiNi_{0.975}Ga_{0.025}O_2$, $LiNi_{0.990}Ti_{0.010}O_2$ and $LiNi_{0.990}Al_{0.005}Ti_{0.005}O_2$ as synthesized and after 50 charge–discharge cycles. $LiNi_{0.975}Ga_{0.025}O_2$ and $LiNi_{0.995}Al_{0.005}O_2$ has the largest crystallite size among the as synthesized samples. $LiNi_{0.975}Ga_{0.025}O_2$ has the largest crystallite size among the samples after 50 charge–discharge cycles. The samples after 50 charge–discharge cycles roughly have larger crystallite sizes than the as synthesized samples.

Figure 11 shows the variations of the strain with the sample $LiNiO_2$, $LiNi_{0.995}Al_{0.005}O_2$, $LiNi_{0.975}Ga_{0.025}O_2$, $LiNi_{0.990}Ti_{0.010}O_2$ and $LiNi_{0.990}Al_{0.005}Ti_{0.005}O_2$ as synthesized and after 50 charge–discharge cycles. $LiNiO_2$ has the largest strain among the as synthesized samples. $LiNiO_2$ has the largest strain among the samples after 50 charge–discharge cycles. The samples after 50 charge–discharge cycles have larger strain than the as synthesized samples.

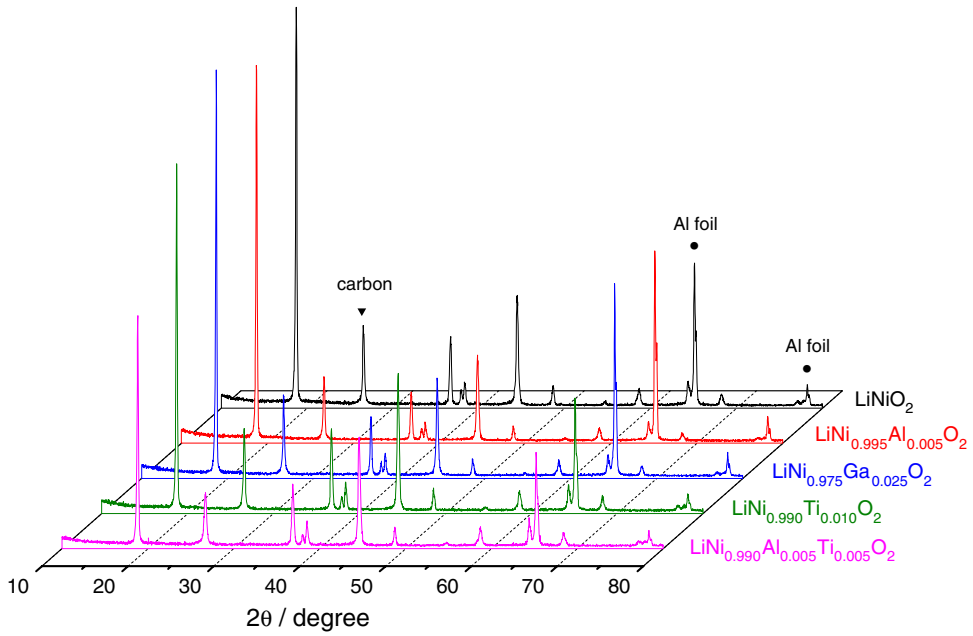

Fig. 8 XRD patterns of the materials after 50 charge–discharge cycles at 0.1 C rate

Table 2 Values of a, c, c/a, unit cell volume, I_{003}/I_{104} and R-factor after 50 charging–discharging cycles at 0.1 C rate for the materials synthesized with excess lithium amount $y = 0.10$ (voltage range 2.7–4.4 V, weight ratio of active material:acetylene black:binder = 85:10:5)

	a/Å	c/Å	c/a	Unit cell volume/Å^3	I_{003}/I_{004}	R-factor $[(I_{006} + I_{102})/I_{101}]$
$LiNiO_2$	2.874	14.205	4.943	101.600	3.639	0.524
$LiNi_{0.995}Al_{0.005}O_2$	2.867	14.214	4.959	101.151	4.417	0.603
$LiNi_{0.975}Ga_{0.025}O_2$	2.870	14.239	4.961	101.584	4.188	0.597
$LiNi_{0.990}Ti_{0.010}O_2$	2.874	14.201	4.941	101.604	2.548	0.486
$LiNi_{0.990}Al_{0.005}Ti_{0.005}O_2$	2.861	14.207	4.966	100.684	2.112	0.555

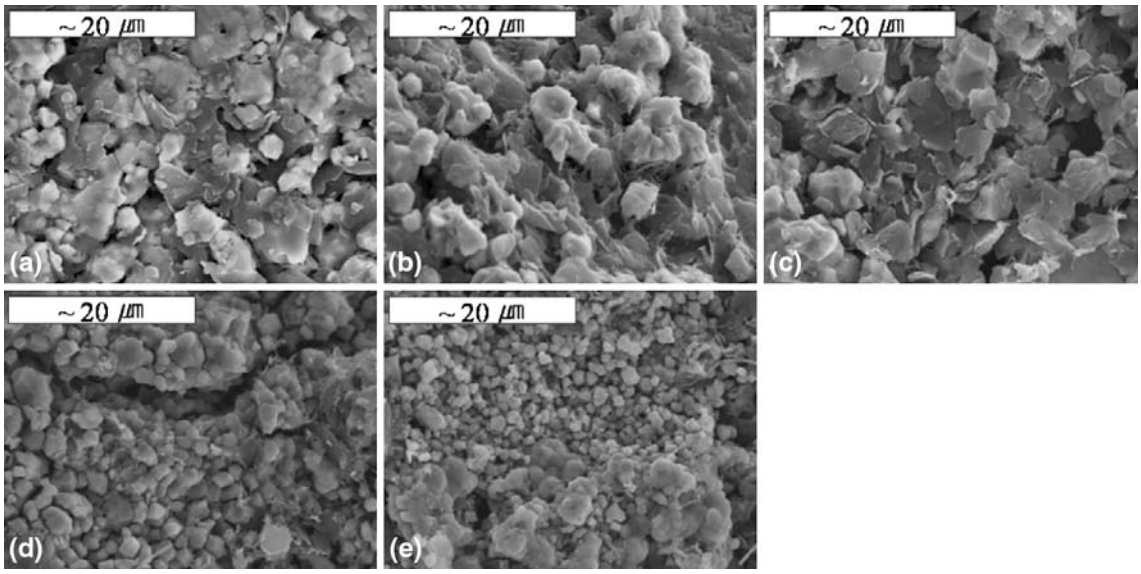

Fig. 9 SEM images after 50 charge–discharge cycles of the materials synthesized with excess lithium amount $z = 0.10$; (**a**) $LiNiO_2$, (**b**) $LiNi_{0.995}Al_{0.005}O_2$, (**c**) $LiNi_{0.975}Ga_{0.025}O_2$, (**d**) $LiNi_{0.990}Ti_{0.010}O_2$ and (**e**) $LiNi_{0.990}Al_{0.005}Ti_{0.005}O_2$

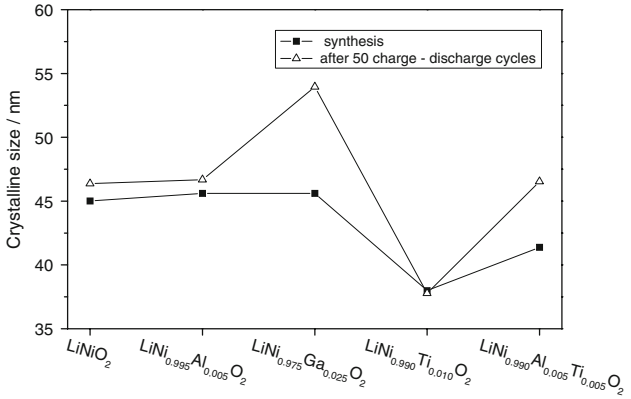

Fig. 10 Variations of the crystallite size with the sample $LiNiO_2$, $LiNi_{0.995}Al_{0.005}O_2$, $LiNi_{0.975}Ga_{0.025}O_2$, $LiNi_{0.990}Ti_{0.010}O_2$ and $LiNi_{0.990}Al_{0.005}Ti_{0.005}O_2$ as synthesized and after 50 charge–discharge cycles

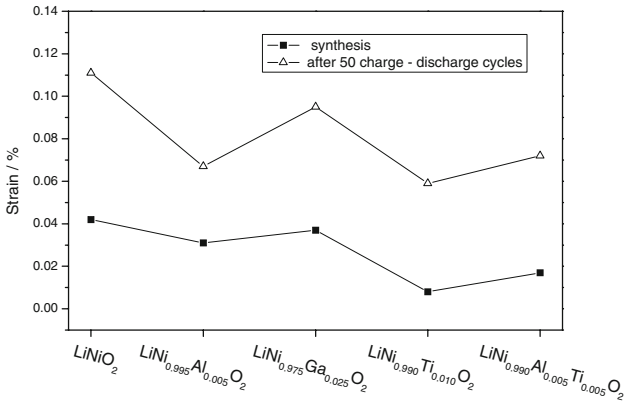

Fig. 11 Variations of the strain with the sample $LiNiO_2$, $LiNi_{0.995}Al_{0.005}O_2$, $LiNi_{0.975}Ga_{0.025}O_2$, $LiNi_{0.990}Ti_{0.010}O_2$ and $LiNi_{0.990}Al_{0.005}Ti_{0.005}O_2$ as synthesized and after 50 charge–discharge cycles

All the synthesized samples $LiNiO_2$, $LiNi_{0.995}Al_{0.005}O_2$, $LiNi_{0.975}Ga_{0.025}O_2$, $LiNi_{0.990}Ti_{0.010}O_2$ and $LiNi_{0.990}Al_{0.005}Ti_{0.005}O_2$ have the α-$NaFeO_2$ structure of the rhombohedral system (space group; $R\bar{3}m$) with no evidence of impurities. $LiNiO_2$ has the largest value of I_{003}/I_{104} and the smallest value of R-factor. This may be related with the results that $LiNiO_2$ has the largest discharge capacity at $n = 20$ and $n = 50$. The variation of the first discharge capacity with the sample has a similar trend to that of the discharge capacity degradation rate with the samples, showing that the sample with a large first discharge capacity has a large discharge capacity degradation rate. $LiNiO_2$ and $LiNi_{0.995}Al_{0.005}O_2$ have a relatively good cycling performance. Roughly speaking, the discharge capacity degradation rate decreases and the discharge capacities at $n = 20$ and $n = 50$ increase as the value of I_{003}/I_{104} increases. The particle sizes of the samples after $n = 50$ are smaller than those before charge–discharge cycling. In particular, the edges of $LiNiO_2$, $LiNi_{0.995}Al_{0.005}O_2$ and $LiNi_{0.975}Ga_{0.025}O_2$ became sharper as compared with the samples before cycling. Cracks are observed on the agglomerates of the particles of $LiNi_{0.990}Ti_{0.010}O_2$. The samples after 50 charge–discharge cycles roughly have larger crystallite sizes than the as synthesized samples. The samples after 50 charge–discharge cycles have larger strain than the as synthesized samples, showing that repetition of intercalation and deintercalation of lithium ions produces strain in the material.

4 Conclusions

The XRD patterns of $LiNiO_2$, $LiNi_{0.995}Al_{0.005}O_2$, $LiNi_{0.975}Ga_{0.025}O_2$, $LiNi_{0.990}Ti_{0.010}O_2$ and $LiNi_{0.990}Al_{0.005}Ti_{0.005}O_2$, synthesized by the combustion method with excess lithium amount $z = 0.10$, have the α-$NaFeO_2$ structure of the rhombohedral system (space group; $R\bar{3}m$) with no evidence of impurities. $LiNi_{0.990}Al_{0.005}Ti_{0.005}O_2$ has the largest first discharge capacity and discharge capacity degradation rate at 0.1 C. These results indicate that the sample with a large first discharge capacity has a large discharge capacity degradation rate. $LiNiO_2$ has the largest discharge capacity at $n = 20$ and $n = 50$. $LiNiO_2$ and $LiNi_{0.995}Al_{0.005}O_2$ have relatively good cycling performances and their discharge capacities at $n = 50$ are 134, 123 mAh/g at 0.1 C rate. As the value of I_{003}/I_{104} increases, roughly speaking, the discharge capacity degradation rate decreases and the discharge capacities at $n = 20$ and $n = 50$ increase. The samples after $n = 50$ has larger crystallite size and strain than those as synthesized.

Acknowledgement This work was supported by Grant No. R01-2003-000-10325-0 from the Basic Research Program of the Korea Science & Engineering Foundation.

References

1. Tarascon JM, Wang E, Shokoohi FK, McKinnon WR, Colson S (1991) J Electrochem Soc 138:2859
2. Armstrong AR, Bruce PG (1996) Lett Nat 381:499
3. Song MY, Ahn DS (1998) Solid State Ion 112:245
4. Ozawa K (1994) Solid State Ion 69:212
5. Alcátara R, Lavela P, Tirado JL, Stoyanova R, Zhecheva E (1997) J Solid State Chem 134:265
6. Peng ZS, Wan CR, Jiang CY (1998) J Power Sources 72:215
7. Dahn JR, von Sacken U, Michal CA (1990) Solid State Ion 44:87
8. Dahn JR, von Sacken U, Juzkow MW, Al-Janaby H (1991) J Electrochem Soc 138:2207
9. Marini A, Massarotti V, Berbenni V, Capsoni D, Riccardi R, Antolini E, Passalacqua B (1991) Solid State Ion 45:143
10. Ebner W, Fouchard D, Xie L (1994) Solid State Ion 69:238
11. Nishida Y, Nakane K, Stoh T (1997) J Power Sources 68:561
12. Morales J, Perez-Vicente C, Tirado JL (1990) Mat Res Bull 25:623
13. Rougier A, Saadoune I, Gravereau P, Willmann P, Delmas C (1996) Solid State Ion 90:83

14. Guilmard M, Rougier A, Grune M, Croguennec L, Delmas C (2003) J Power Sources 115:305
15. Song MY, Lee R, Kwon IH (2003) Solid State Ion 156:319
16. Chang SH, Kang SG, Song SW, Yoon JB, Choy JH (1996) Solid State Ion 86–88:171
17. Guilmard M, Croguennec L, Delmas C (2003) J Electrochem Soc 150(10):A1287
18. Reimers JN, Rossen E, Jones CD, Dahn JR (1993) Solid State Ion 61:335
19. Kanno R, Shirane T, Inaba Y, Kawamoto Y (1997) J Power Sources 68:145
20. Kim HU, Youn SD, Lee JC, Park HR, Park CG, Song MY (2005) J Korean Ceram Soc 42(9):631
21. Kim HU, Youn SD, Lee JC, Park HR, Song MY (2005) J Korean Ceram Soc 42(5):352
22. Song MY, Kwon IK, Kim HU, Shim S, Mumm DR (2006) J Appl Electrochem 36:801
23. Ohzuku T, Ueda A, Nagayama M (1993) J Electrochem Soc 140:1862
24. Suryanarayana C, Grant Norton M (1998) X-ray diffraction: a practical approach. Plenum Press, New York, pp 207–222